Expression, Purification, and Characterization of *Bacillus subtilis* Cytochromes P450 CYP102A2 and CYP102A3: Flavocytochrome Homologues of P450 BM3 from *Bacillus megaterium*†

Mattias C. U. Gustafsson,‡ Olivier Roitel,§ Ker R. Marshall,§ Michael A. Noble,|| Stephen K. Chapman,⊥ Antonio Pessegueiro,▽ Armand J. Fulco,▽ Myles R. Cheesman,∞ Claes von Wachenfeldt,‡ and Andrew W. Munro*,§

Department of Cell and Organism Biology, Lund University, Sölvegatan 35, SE-223, 62 Lund, Sweden, Department of Biochemistry, University of Leicester, The Adrian Building, University Road, Leicester LE1 7RH, United Kingdom, Anadys Pharmaceuticals Inc., 6777 Nancy Ridge Drive, San Diego, California 92122, Department of Chemistry, University of Edinburgh, The King's Buildings, West Mains Road, Edinburgh EH9 3JJ, United Kingdom, Department of Biological Chemistry, University of California Los Angeles School of Medicine, P.O. Box 951737, Los Angeles, California 90095-1737, and School of Chemical Sciences, University of East Anglia, Norwich NR4 7TJ, United Kingdom

Received October 24, 2003; Revised Manuscript Received March 9, 2004

ABSTRACT: The *cyp102A2* and *cyp102A3* genes encoding the two *Bacillus subtilis* homologues (CYP102A2 and CYP102A3) of flavocytochrome P450 BM3 (CYP102A1) from *Bacillus megaterium* have been cloned, expressed in *Escherichia coli*, purified, and characterized spectroscopically and enzymologically. Both enzymes contain heme, flavin adenine dinucleotide (FAD) and flavin mononucleotide (FMN) cofactors and bind a variety of fatty acid molecules, as demonstrated by conversion of the low-spin resting form of the heme iron to the high-spin form induced by substrate-binding. CYP102A2 and CYP102A3 catalyze the fatty acid-dependent oxidation of reduced nicotinamide adenine dinucleotide phosphate (NADPH) and reduction of artificial electron acceptors at high rates. Binding of carbon monoxide to the reduced forms of both enzymes results in the shift of the heme Soret band to 450 nm, confirming the P450 nature of the enzymes. Reverse-phase high-performance liquid chromatography (HPLC) of products from the reaction of the enzymes with myristic acid demonstrates that both catalyze the subterminal hydroxylation of this substrate, though with different regioselectivity and catalytic rate. Both P450s 102A2 and 102A3 show kinetic and binding preferences for long-chain unsaturated and branched-chain fatty acids over saturated fatty acids, indicating that the former two molecule types may be the true substrates. P450s 102A2 and 102A3 exhibit differing substrate selectivity profiles from each other and from P450 BM3, indicating that they may fulfill subtly different cellular roles. Titration curves for binding and turnover kinetics of several fatty acid substrates with P450s 102A2 and 102A3 are better described by sigmoidal (rather than hyperbolic) functions, suggesting binding of more than one molecule of substrate to the P450s, or possibly cooperativity in substrate binding. Comparison of the amino acid sequences of the three flavocytochromes shows that several important amino acids in P450 BM3 are not conserved in the *B. subtilis* homologues, pointing to differences in the binding modes for the substrates that may explain the unusual sigmoidal kinetic and titration properties.

The cytochromes P450 are a ubiquitous family of monooxygenases that play key roles in mammalian xenobiotic, steroid, and lipid metabolism (*1*). They catalyze the reductive scission of molecular oxygen, with one atom of oxygen being reduced to water and the other used to hydroxylate the substrate. Two electrons are delivered from NAD(P)H[1] via flavoprotein and/or iron−sulfur redox partners (*2*). The two protons required for the production of water appear to be delivered from bulk solvent via a specific channel in the P450 active site (*3*). Eukaryotic P450s are almost invariably membranous and interact with reductase partners at the membrane surface (*4*). By contrast, bacterial P450s and their redox partners are soluble enzymes, providing simpler systems for structural and biophysical studies (*2*). The first

† This work was funded by the Biotechnology and Biological Sciences Research Council (U.K.) (grants to A.W.M. and S.K.C.), the Crafoord Foundation and The Royal Swedish Academy of Sciences (grant to C.V.W.) and the European Community Improving Human Potential program through a Marie Curie Fellowship under Contract HPMF-CT-2002-01633 to O.R. M.C.U.G. was supported by a travel fellowship from the Kungliga Fysiografiska Sällskapet in Lund.

* Author to whom correspondence should be addressed: phone 0044 116 252 3464; fax 0044 116 252 3369; e-mail awm9@le.ac.uk.

‡ Lund University.

§ University of Leicester.

|| Anadys Pharmaceuticals Inc.

⊥ University of Edinburgh.

▽ UCLA School of Medicine.

∞ University of East Anglia.

[1] Abbreviations: P450 BM3/CYP102A1, flavocytochrome P450 BM3 from *Bacillus megaterium*; CYP102A2 and CYP102A3, P450 BM3 homologues from *Bacillus subtilis*, 2′-AMP, 2′-adenosine monophosphate; 2′-ADP, 2′-adenosine diphosphate; DEAE, diethylaminoethyl; FAD, flavin adenine dinucleotide; FMN, flavin mononucleotide; NAD(P)H, reduced nicotinamide adenosine dinucleotide (phosphate); PCR, polymerase chain reaction.

10.1021/bi035904m CCC: $27.50 © 2004 American Chemical Society
Published on Web 04/16/2004

P450 atomic structure solved was for the soluble camphor hydroxylase P450cam (CYP101) from *Pseudomonas putida* (*5*), and all but two of the P450 atomic structures solved subsequently have been from soluble bacterial P450s. A breakthrough was made with the determination of the structure of a modified rabbit CYP2C5, the first mammalian P450 structure (*6*). However, this was achieved only after extensive protein engineering to discourage aggregation and promote solubility (*7*). Clearly, this points the way to future successes in determination of the structures of eukaryotic P450s, as evidenced by the structures of substrate complexes of rabbit CYP2C5 and human CYP2C9 (*8*, *9*). However, arguably the most important structures have been those of the substrate-free and palmitoleate-bound forms of the heme domain of P450 BM3 from *Bacillus megaterium*, a high-activity fatty acid hydroxylase in which the redox partner (an FAD- and FMN-containing NADPH−cytochrome P450 reductase) is fused to the P450 in a single polypeptide (*10*−*12*). Virtually all other bacterial P450s operate a class I reductase system, with electrons (often from NADH rather than NADPH) delivered from a ferredoxin, which is itself reduced by a separate FAD-containing ferredoxin reductase (*2*, *13*). P450 BM3 uses instead a class II-type diflavin reductase system, akin to most eukaryotic P450s and mammalian drug-metabolizing P450 systems. Thus, P450 BM3 has been studied as a good model for the analysis of structure/function relationships in the mammalian-type P450/P450 reductase system (*14*).

P450s are considered to be relatively rare in prokaryotes and for some years were thought to be required in bacteria only as components of pathways designed for the breakdown of unusual carbon compounds (e.g., camphor and terpenes) as energy sources (*5*, *15*). Indeed, the fact that there are no P450s in the gram-negative bacterium *Escherichia coli* contrasts with the sequence of the model plant *Arabidopsis thaliana*, which contains more than 200 P450 and P450-like gene sequences. This indicates that P450 activity is not essential for certain bacteria but fundamental to eukaryote physiology (*16*, *17*). However, the recent genome sequence of the pathogenic bacterium *Mycobacterium tuberculosis* (*18*), and those of other mycobacteria and streptomycetes indicate that these bacteria encode large numbers of P450s (20 in the case of *M. tuberculosis*) and suggest that the P450s play crucial roles in the metabolism of certain bacteria (*19*). Although P450s are apparently absent from the model gram-negative bacterium *E. coli*, the genome sequence of the gram-positive model organism *Bacillus subtilis* 168 encodes eight cytochromes P450 (*20*, *21*).

Of these *B. subtilis* P450s, two have been well-characterized at the enzyme level. BioI (CYP107H1) is involved in the early stages of synthesis of the vitamin biotin, and has been reported both to catalyze the acyl bond cleavage of long-chain fatty acyl CoA molecules and to hydroxylate long-chain fatty acids (*22*−*24*). CYP152A1 (P450 BSβ) has been structurally characterized and catalyzes hydrogen peroxide-dependent hydroxylation of long-chain fatty acids (*25*, *26*). However, two other *B. subtilis* P450s (CYP102A2 and CYP102A3) show obvious similarity at the predicted amino acid level to CYP102A1 (flavocytochrome P450 BM3) from *B. megaterium*—a fatty acid hydroxylase P450:P450 reductase fusion enzyme of mechanistic and biotechnological importance in the P450 superfamily (*10*, *12*, *14*).

Proteins containing both flavin and heme in a single polypeptide are relatively rare in nature but include the lactate dehydrogenase flavocytochrome b_2 from *Saccharomyces cerevisiae* (*27*), the fumarate reductase flavocytochrome c_3 from *Shewanella frigidimarina* (*28*), and bacterial flavohemoglobin (*29*). Proteins containing each of the cofactors FAD, FMN, and heme are rarer still, and the first of these to be discovered was flavocytochrome P450 BM3 (*30*). Subsequently, the various isoforms of nitric oxide synthase were shown to have a similar domain structure to P450 BM3 and to contain the same cofactor complement (and, in addition, tetrahydrobiopterin) (*31*). More recently, a further membrane-associated diflavocytochrome P450 has been isolated from the fungus *Fusarium oxysporum* (P450foxy, CYP505A1) (*32*). Here, we report the cloning, expression, and characterization of the two further flavocytochromes P450 from *B. subtilis*, along with the demonstration that they bind a range of long-chain fatty acid substrates and catalyze their hydroxylation. The substrate preference profiles of these P450s, and aspects of their substrate binding and kinetic properties, are different from those of P450 BM3. These data, along with important substitutions of amino acids known to be functionally important in P450 BM3, suggest that there are important structural differences between these enzymes and that the *B. subtilis* flavocytochromes P450 may be implicated in the processing of long-chain unsaturated and branched-chain fatty acids *in vivo*.

EXPERIMENTAL PROCEDURES

General Molecular Techniques. Chromosomal DNA was prepared from *B. subtilis* strain 1A1 (*trpC2*) (obtained from Bacillus Genetic Stock Center, Columbus, Ohio: http://www.bgsc.org/) according to the method described by Hoch (*33*). *E. coli* strains XL1-Blue (*recA1 endA1 gyrA96 thi-1 hsdR17 supE44 relA1 lac* [FΦ*proAB lacI*^{q}ZΔM15 Tn10-(Tc^R)]) (Stratagene) and BL21(DE3) (F$^-$ *hsdS* (r_B^- m_B^-) *dcm ompT gal* λDE3) (*34*) were used for general DNA manipulation and gene expression, respectively. *E. coli* cells were transformed by electroporation, as described previously (*35*).

Cloning of the cyp102A2 and cyp102A3 Genes. The *cyp102A2* (*yetO*) gene was amplified by PCR using oligonucleotide primers 102A21 and 102A22 and *B. subtilis* 1A1 chromosomal DNA template. The sequence of 102A21 (5′-CCCTCTAGAGGGAGGTATGGTTCGATGAAGGAAACAAGCC-3′) includes a *Xba*I site (underlined) near the 5′ end, followed by 30 nucleotides containing a ribosome binding site and the 5′-coding sequence of *cyp102A2*. The sequence of 102A22 (5′-CCCTCGAGTCTTCTTTATCTATATCCCTGC-3′) includes a XhoI site followed by nucleotides complementary to the extreme 3′ end of CYP102A2 coding sequence. The PCR product was purified and digested with *Xba*I and *Xho*I. The cut PCR fragment was introduced into the corresponding sites of plasmid pBluescript II SK(−) to yield plasmid pBSCyp102A2. The integrity of the cloned *cyp102A2* gene was verified by DNA sequencing.

The *cyp102A3* (*yrhJ*) gene was cloned in a similar way by use of oligonucleotides YrhI6 and YrhJ2. The sequence of YrhI6 (5′- GGACGCCATTAAGCTTCATTCATCAC-3′) includes the extreme 3′ end of the adjacent *yrhI* coding sequence that contains a *Hin*dIII site. The sequence (5′-

CCCTCGAGGCCGACCATTCGGCTGATTCAT-3′) of the YrhJ2 primer includes a *Xho*I site (underlined) followed by 22 nucleotides complementary to the 3′ noncoding region of the *cyp102A3* gene. The PCR product was purified and digested with *Hin*dIII and *Xho*I. The cut PCR fragment was introduced into the corresponding sites of plasmid pBluescript II SK(−) to yield plasmid pBSCyp102A3. The integrity of the cloned *cyp102A3* gene was verified by DNA sequencing.

The *cyp102A2* gene in pBSCyp102A2 and the *cyp102A3* gene in pBSCyp102A3 were then excised from these plasmids by *Sac*I/*Xho*I and *Hin*dIII/*Xho*I digestion, respectively, and subcloned into the expression plasmid pET21-(+) (Novagen) predigested with *Sac*I/*Xho*I and *Hin*dIII/*Xho*I, respectively, under control of the phage T7 promoter. The resulting plasmids were named pETCyp102A2 and pETCyp-102A3, respectively, and were used for production of the flavocytochrome enzymes.

Gene Expression. Plasmids pETCyp102A2 and pETCyp-102A3 were introduced into *E. coli* strain BL21(DE3), in which expression of the T7 RNA polymerase gene is under control of the *lac* promoter. The resulting strains were grown at 37 °C in Terrific broth containing ampicillin (100 mg/L) with vigorous agitation (250 rpm) until the cultures reached an absorbance at 600 nm of 0.5. Typically, cultures of 10 L were grown. Following a further 15 min incubation at 30 °C, expression of the P450 enzymes was induced by the addition of 0.5 mM isopropyl β-D-thiogalactopyranoside (IPTG), and growth of the culture was continued at 30 °C with shaking at approximately 200 rpm. The cells were harvested 7 h later by centrifugation at 5000*g* for 10 min at 4 °C.

Protein Purification. Flavocytochromes P450 102A2 and 102A3 were prepared in identical fashion, by a method similar to that described previously for P450 BM3 (*35*). Cells of BL21(DE3) expressing the P450s were washed by resuspension in ice-cold 50 mM Tris-HCl (pH 7.4) containing 1 mM ethylenediaminetetraacetic acid (EDTA) (buffer A). Protease inhibitors [benzamidine hydrochloride and phenylmethanesulfonyl chloride (PMSF) at 1 mM] were also added. Cells were pelleted by centrifugation as previously and then frozen at −80 °C to weaken cell walls. Cells were next thawed and resuspended in a small volume (~200 mL) of ice-cold buffer A including protease inhibitors. Cells were broken by sonication with an MSE Soniprep sonicator on 80% power. Ten bursts of sonication for 15 s were given, with 1 min intervals between bursts. Cells were kept on ice throughout to minimize proteolysis. Following sonication, the extract was separated from cellular debris by centrifugation at 18000*g* for 45 min. The soluble extract was removed and dialyzed extensively into buffer A, prior to loading onto a DEAE Sephacel (Pharmacia) column (5 cm × 40 cm) preequilibrated in the same buffer. The P450s bound as a tight red band at the top of the resin. Proteins were eluted with a linear gradient of potassium chloride in buffer A (0−500 mM over 500 mL), and the P450s were eluted between 100 and 250 mM salt. The reddest colored fractions containing the highest quantities of P450 were pooled and desalted by exhaustive dialysis into buffer A, as previously. Thereafter, proteins were loaded onto a 2′,5′-ADP-agarose column (Sigma, column dimensions 1 cm × 10 cm) preequilibrated in buffer A. Again, a tight red band was seen to form at the top of the column. The column was washed extensively (10 column volumes) with buffer A, and then the P450s were eluted with the same buffer containing either $NADP^+$ (5 mM) or 2′-AMP (10 mM). Eluted P450 was concentrated by ultrafiltration (Centriprep and Centricon 100 000 molecular weight cut-off concentrators, Millipore) to volumes of less than 2 mL and dialyzed extensively into buffer A to remove the residual $NADP^+$/2′-AMP. When necessary, a final chromatography step, to remove minor protein contaminants, was performed on Q-Sepharose resin (Pharmacia) under the same binding and elution conditions described for the DEAE column above. All operations were performed at 4 °C. Finally, pure P450s were dialyzed twice against 500 mL of buffer A containing glycerol (50% v/v) and protease inhibitors prior to storage at −80 °C. Enzymes were used within 1 month of manufacture.

Spectroscopic and Kinetic Characterization of P450s. UV−visible absorption spectra of the purified P450s were recorded on a Shimadzu UV-2401 scanning spectrophotometer or a Varian Cary UV-50 Bio in quartz cuvettes of path length 1 cm. Protein concentrations used for spectral measurements and for spectrophotometric titrations with substrates and ligands to the heme iron were in the range of 1−5 μM, and these were performed at 30 °C in buffer B [20 mM 3-(*N*-morpholino)propanesulfonic acid (MOPS) (pH 7.4) plus 100 mM KCl], shown previously to produce good activity for the P450 BM3 enzyme (e.g., *36*). Reduction of the P450s was achieved by addition of a few grains of solid sodium dithionite to buffered enzyme solutions, and formation of the carbon monoxide complexes of CYP102A2 and CYP102A3 was achieved by slow bubbling of carbon monoxide gas into the reduced enzyme solutions for approximately 1 min. Difference spectra were generated by subtraction of the spectrum for the reduced form from that of the carbon monoxide ligated form. Concentration of P450 was determined by the method of Omura and Sato (*37*), with the coefficient $\epsilon_{450-490} = 91\,000\ M^{-1}\ cm^{-1}$ being used for the absorption difference between 450 and 490 nm in the reduced/CO minus reduced spectrum. The presence and relative quantities of FAD and FMN cofactors in flavocytochrome enzymes were established by a fluorometric method (*38*).

Spectral determinations of the K_d values for the binding of fatty acid substrates to the P450s were performed as described previously (e.g., *36*, *39*), by addition of small volumes (<5 μL total) of fatty acids to stock solutions of the CYP102A2 or CYP102A3 solutions (typically 1−5 μM in buffer B) at 30 °C by use of a 10 mL Hamilton gas-tight syringe (Hamilton, Reno, NV). Stock solutions of fatty acid substrates for the P450s were made up either as ethanolic stocks (25 or 50 mM) or as saturated aqueous solutions in buffer B and were maintained at 30 °C prior to assay. Spectral differences due to the perturbation of the spin-state equilibrium of the heme iron in favor of the high-spin form were observed (i.e., a shift of the heme Soret maximum toward ~390 nm), and absorption difference spectra were generated at each point in the titrations by subtraction of the spectrum for the resting (fatty acid-free) species from those at subsequent titration points. The K_d values were determined by plotting the maximal absorption changes calculated from each difference spectrum against the concentration of the substrate and fitting the data to appropriate

Table 1: Characteristic Retention Times and Fragmentation Patterns of Myristic Acid Metabolites Used to Identify Position of Substrate Hydroxylation[a]

site of hydroxylation	retention time (min)	*m/z* of fragment		
		$M - CH_3(CH_2)_{n-1}$	$M - CH_3(CH_2)_{n-1} - CH_3OH$	$M - CH_3(CH_2)_{n-1} - CHO$
ω-1	24.66	243	211	214
ω-2	24.54	229	197	200
ω-3	24.23	215	183	186

[a] Retention times and masses for the fragments of the three hydroxylated derivatives of myristic acid produced by P450 BM3 (as described in Experimental Procedures) are shown.

functions by use of Origin software (Microcal). For P450 BM3 (CYP102A1), the data for binding of all fatty acids tested to date are described best by a rectangular hyperbola, describing single-site, reversible binding. This is also the case for certain substrates for CYP102A2 and CYP102A3. However, data for the binding of various substrates for the *B. subtilis* flavocytochromes were nonhyperbolic, describing more closely sigmoidal curves. To estimate the apparent binding constant (K) in these cases, data were fitted to the Hill equation: $A = A_{max}S^H/(K^H + S^H)$, where A is the absorption difference observed at each titration point, A_{max} is the maximal absorption difference at substrate saturation, S is the substrate concentration, K is the substrate concentration at 50% of the final overall change, and H is the Hill coefficient. In fitting nonhyperbolic data to this equation, only the value of K was considered relevant as a measure of the apparent binding constant for substrate, since we consider that the nonhyperbolic curves may not reflect cooperativity between binding of distinct substrate molecules in most or all of the cases examined (see Discussion).

Kinetic assays of fatty acid-dependent NADPH oxidation were performed at 30 °C in buffer B, as described previously (*36*). Initial rates of fatty acid-induced NADPH oxidation were measured by monitoring the absorption change at 340 nm ($\epsilon_{340} = 6210\ M^{-1}\ cm^{-1}$), and NADPH was maintained at saturating concentration (200 μM) in the assay. Fatty acids were prepared as described above and added in the concentration range between 0 and 1 mM, according to the affinity of the enzyme for the fatty acid. Enzymes (CYP102A2 and CYP102A3) were typically in the concentration range 10−100 nM, and the reaction was initiated by the addition of NADPH. Rates of A_{340} change were converted into activity units (moles of NADPH oxidized per minute per mole of enzyme) and plotted against fatty acid substrate concentration. At least three replicate experiments were performed at each substrate concentration. As described above, some data sets described rectangular hyperbolae (as seen for P450 BM3 with all substrates to date) and were fitted to the Michaelis function to obtain the K_M and k_{cat} parameters. Other data sets were nonhyperbolic, and apparent values for the maximal rate constant (k_{max}) and binding coefficient (K_H) were estimated from the Hill function.

Assays for reductase domain-dependent electron transfer to exogenous electron acceptors (cytochrome *c* or ferricyanide) were also performed at 30 °C in buffer B, with approximately 1−5 nM enzyme, NADPH at 200 μM, and electron acceptors across the appropriate concentration range for their K_M values (cytochrome *c* from 0 to 200 μM; ferricyanide from 0 to 2 mM). As above, reactions were initiated by addition of NADPH, and absorption change versus time recorded for cytochrome *c* at 550 nm ($\Delta\epsilon_{550} = 22\ 640\ M^{-1}\ cm^{-1}$) and for ferricyanide at 420 nm ($\Delta\epsilon_{420} = 1020\ M^{-1}\ cm^{-1}$). Observed rate constants, k_{obs}, were plotted versus [electron acceptor] and were fitted to a rectangular hyperbola to define k_{cat} and K_M parameters.

EPR Spectroscopy. Electron paramagnetic resonance (EPR) spectra were recorded on an X-band ER-200B spectrometer (Bruker Spectrospin) interfaced to an ESP1600 computer and fitted with a liquid helium flow-cryostat (ESR-9, Oxford Instruments). Spectra were recorded at 10 K with 2 mW microwave power and a modulation amplitude of 1 mT. Protein samples (~200 μM) were in 50 mM Tris-HCl (pH 7.2).

Determination of Products from CYP102A2 and CYP102A3 Turnover of Myristic Acid. The products of the catalytic turnover of myristic acid (tetradecanoic acid) by P450 BM3 and flavocytochromes P450 102A2 and 102A3 were determined by high-performance liquid chromatography (HPLC) and gas chromatography/mass spectrometry (GC/MS) according to the method outlined previously (*40*). A Hewlett-Packard 5971A GC/MS instrument utilizing electron impact ionization (70 eV) was used to determine structural information on the monohydroxylated metabolites of myristic acid. Metabolites were generated by incubation of 120 μM myristic acid in the presence of 5 mM NADPH and a catalytic amount of the P450s (1 nM) in a 2 mL volume of 100 mM potassium phosphate (pH 8.0) for up to 3 h. Samples were taken after 20 min and at the end of the incubation period. The metabolites were extracted into diethyl ether and converted to their methyl ester derivatives by diazomethane, before analysis on the GC/MS. Chromatography of the samples was performed on a HP-35 capillary column (30 m × 0.25 mm i.d. × 0.25 μM film thickness) with a thermal gradient beginning at 100 °C for 0.5 min and increasing to 200 °C at a rate of 5 °C/min for 5 min and then to a final temperature of 250 °C at a rate of 10 °C/min. Injector temperature was set to 250 °C and the GC/MS transfer line was set at 280 °C. Column flow rate was set at 0.76 mL/min.

The mass spectra of the products from the control run (P450 BM3) were used to identify each GC peak. Monohydroxylated products were identified by their characteristic fragmentation pattern as shown in Table 1. The distribution of products was based on the relative peak area of the gas chromatogram, in which the total ion current was used to assess quantity.

Other Methods. Alignment of amino acid sequences was done with the ClustalW program via the European Bioinformatics Institute website at http://www.ebi.ac.uk/clustalw/.

RESULTS

Amino Acid Sequence Comparisons with P450 BM3. The prototype enzyme for P450/P450 reductase fusions of the

FIGURE 1: (A) Amino acid sequence alignment of the heme domain of CYP102A1 (residues 1−472 of *B. megaterium* flavocytochrome P450 BM3) with the respective domains of *B. subtilis* CYP102A2 and -102A3. (B) Amino acid sequence alignment of the reductase domain of CYP102A1 (residues 472−1048) of *B. megaterium* flavocytochrome P450 BM3) with the respective domains of *B. subtilis* CYP102A2 and -102A3. Alignments were performed with the ClustalW package, as described in Experimental Procedures. (★) Identical residues in the different enzymes; (:) conserved substitutions; (.) semiconserved substitutions.

CYP102A2 and CYP102A3 class is flavocytochrome P450 BM3 (CYP102A1) from *B. megaterium*. The high degree of relatedness between these enzymes is evident from the amino acid alignments of their heme (P450) and diflavin (P450 reductase) domains shown in Figure 1, left and right panels, respectively. The overall levels of amino acid identity across the three flavocytochromes are high. There is 48.7% sequence identity between the three full-length enzymes (with 59.8% identity between P450 BM3 and CYP0102A2, 58.4% identity between P450 BM3 and CYP0102A3, and 60.9% identity between CYP102A2 and CYP0102A3 in pairwise alignments). The most obvious difference in the alignments is seen with the apparent insertion of approximately 7−8 residues in the CYP102A2 sequence (residues 482−488/489) relative to P450 BM3 and CYP102A3 (Figure 1, right panel). This region of the sequence corresponds to the structurally undefined linker region between the heme and FMN domains of the enzymes. The sequence diversity observed in this region (particularly in view of the rapid turnover kinetics of the enzymes reported below) may reflect that changes in linker constitution (particularly extended length) are compatible with the retention of efficient interdomain electron transfer in these systems.

Extensive structural and protein engineering studies on the heme domain of P450 BM3 over the past decade have revealed roles for a number of amino acids in catalysis and substrate/cofactor binding (*14*). Several of these residues are conserved in the heme domains of CYP102A2 and CYP-102A3, including Phe 87 in P450 BM3 (Phe 89 in CYP102A2 and CYP102A3) that interacts with the ω-terminus of fatty acid substrates and prevents hydroxylation at this position (*11*, *41*); Trp 96 (Trp 98 in CYP102A2 and CYP102A3) that interacts with heme propionate and affects heme binding and spin-state equilibrium of bound heme (*10*, *42*); Cys 400 (Cys 403 in CYP102A2 and CYP102A3) that provides the proximal ligand to the P450 heme iron; and Phe 393 (Phe 396 in CYP102A2 and CYP102A3) that interacts with the Cys 400−Fe bond and regulates reduction potential of the heme iron (*43*). Other completely conserved residues (numbers for P450 BM3) include Leu 75, Leu 181, Ile 263, and Leu 437, which have been implicated in control of substrate binding and selectivity (*36*, *44*). The composition of several structural elements is strongly conserved, with extended identity particularly obvious in the I helix, which contains several residues of importance to substrate binding and catalysis in P450 BM3 (*14*). However, some important sequence variations are obvious. Sligar and co-workers (*45*) showed that a P25Q mutant of P450 BM3 exhibited dramatically weakened binding of palmitic acid, and this residue is replaced by a leucine (Leu 27) in CYP102A3. Residues Arg 47 and Tyr 51 are recognized as important for P450 BM3's interaction with the carboxylate group of fatty acids, although a Y51F mutant has minimal effects on catalytic efficiency (*11*, *36*). Neither amino acid is conserved in the *B. subtilis* flavocytochromes: CYP102A2 has Gly 49 and Val 53 and CYP102A3 has Val 49 and Phe 53 instead. The P450 BM3 heme domain (residues 1−472 of the flavocytochrome) shows a slightly higher level of identity with CYP012A3's heme domain (65.0%) than with that of CYP102A2 (63.8%), with a slightly higher level of identity observed between the two *B. subtilis* heme domains (65.7%).

In the reductase domains (residues 473−1048 in P450 BM3), levels of amino acid sequence identity are slightly lower than in the heme domains (56.8% between P450 BM3 and CYP102A2, 53.3% between P450 BM3 and CYP102A3, and 57.0% between CYP102A2 and CYP102A3). As with the heme domain, several catalytically important residues are retained. These include the "catalytic triad" of residues involved in efficient hydride transfer reaction from NADPH to FAD in the diflavin reductase family (*46*, *47*) comprising Ser 830, Cys 999 and Asp 1044 in P450 BM3 (Ser 843/835, Cys 1011/1004, and Asp 1056/1049 in CYP102A2/CYP102A3, respectively) and the FMN-interaction residues Gly 570 (Gly 581/574) and Trp 574 (Trp 585/578) (*48*). In contrast to the results for the heme domains, P450 BM3's reductase domain shows a higher level of amino acid sequence identity to the CYP102A2 reductase (56.8%) than to the CYP102A3 reductase (53.3%). CYP102A2 and CYP102A3 reductases are 56.99% identical.

Cloning and Expression of P450s. The genes encoding cytochromes P450 102A2 and 102A3 were amplified from *B. subtilis* genomic DNA by PCR. DNA sequence of the genes was verified against that from the genome sequence by automated Sanger sequencing (*49*). The P450 genes were cloned into expression vector pET21(+), creating expression plasmids pETCyp102A2 and pETCyp102A3. Expression tests in various *E. coli* T7 RNA polymerase lysogenic strains revealed consistently high levels of enzyme production, with expression cell pastes developing a red color due to overproduction of the cytochromes and bands of the appropriate mass (ca. 120 kDa in both cases) clearly visible by sodium dodecyl sulfate−polyacrylamide gel electrophoresis (SDS−PAGE) analysis (not shown). Expression for protein purification was done with BL21(DE3)/pETCyp102A2 and BL21(DE3)/pETCyp102A3, with growth and induction as described in Experimental Procedures. Enzymes were purified to homogeneity by a strategy similar to that previously employed for the *B. megaterium* P450 BM3 enzyme, involving anion-exchange chromatography (DEAE-Sepharose) and affinity for 2′,5′-ADP−agarose, with a final anion-exchange step on Q-Sepharose resin for preparation of ultrapure enzymes (*36*, *50*). Both proteins were prepared in good yield from the *E. coli* expression system (typically up to 15% of total cell protein, a level similar to that found previously for the P450 BM3 enzyme; *50*). However, while CYP102A3 consistently had a full complement of bound heme, preparations of CYP102A2 usually contained a mixture of holo- and apoprotein. Heme content for CYP102A2 was typically in the range of 50−80%, with occasional preparations having near-stoichiometric heme incorporation (see below). Alteration of growth conditions (temperature, culture time, induction levels) did not have a significant effect on the level of heme incorporation in the T7 expression system. Moreover, the lowered content of heme for CYP102A2 was observed at the cell lysate stage (by comparison of the CYP102A2 heme and flavin absorption components, relative to those for P450 BM3 and CYP102A3 at the same stage), indicating that there is a lowered efficiency of heme incorporation in the CYP102A2 enzyme, as opposed to heme loss occurring during enzyme purification. A similar level of heme incorporation was noted previously for various tryptophan 96 mutants of P450 BM3 (*42*). However, this amino acid is conserved in both CYP102A2 and CYP102A3. Evidently heme incorporation is less efficient for the CYP102A2 enzyme in the *E. coli* expression system.

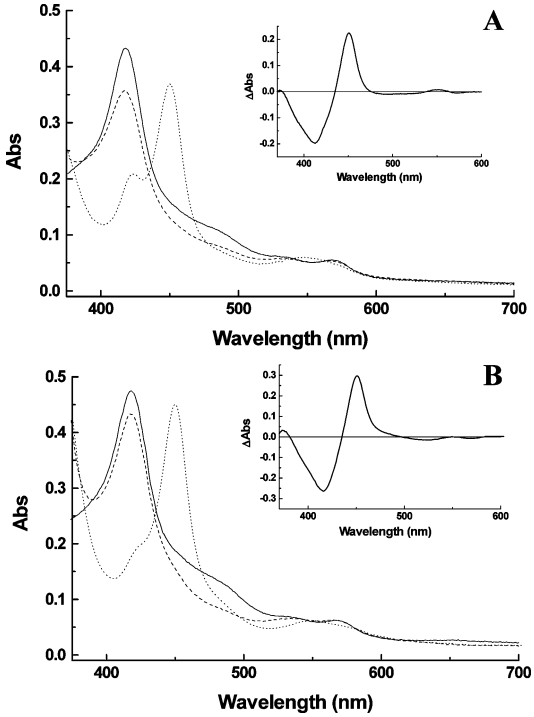

FIGURE 2: Spectral features of CYP102A3 (4.1 μM, panel A) and CYP102A2 (4.4 μM, panel B). Spectra are shown for the oxidized (solid line), sodium dithionite-reduced (dashed line), and reduced/carbon monoxide-bound (dotted line) forms of the enzymes. Sodium dithionite completely reduces the flavins in both enzymes, leading to spectral bleaching. Binding of carbon monoxide results in the formation of Fe^{2+}-CO complexes with heme Soret absorption maxima shifted to 450 nm in both cases. Insets show difference spectra generated by subtraction of the relevant dithionite-reduced spectra from those for the carbonmonoxy complexes.

Spectral Characterization: (A) Oxidized, Reduced, and CO-Bound Spectra. The UV−visible spectra of oxidized CYP102A2 and CYP102A3 enzymes showed expected features for flavocytochrome homologues of P450 BM3, with absorption components for both heme and flavin cofactors evident (Figure 2). The absorption maxima for the heme Soret bands are located at 418 nm for both enzymes, with broad absorption features on either side of the Soret bands due to flavin (FAD and FMN) in the enzymes. The smaller α and β absorption bands are located at approximately 567 and 535 nm for both CYP102A2 and CYP102A3. Addition of small amounts of sodium dithionite induced complete reduction of the flavins to their hydroquinone forms, leading to diminished intensity of the absorption in the visible region. However, the position of the heme Soret maximum was virtually unchanged, indicating that this cofactor remained completely oxidized on addition of dithionite under aerobic conditions. This is likely to reflect the rapid reaction of ferrous P450 heme iron with oxygen in CYP102A2 and CYP102A3, which regenerates the ferric heme iron, as seen previously with P450 BM3 (*51*). Addition of carbon monoxide (CO) to the dithionite-reduced enzymes results in ligation of the CO to the ferrous heme iron, forcing the equilibrium across to the Fe^{2+}−CO complex. For both CYP102A2 and CYP102A3, this results in the movement of the Soret band to 450 nm (as expected for a P450 enzyme)

and the formation of a single spectral feature in the α/β band region at ~550 nm (Figure 2). Subtraction of the spectra of reduced CYP102A2/A3 from those for the ferrous−CO complexes produced difference spectra typical for cytochrome P450 enzymes, with peak maxima and trough minima at 450.5 ± 0.5 nm and 415 ± 2 nm (Figure 2, insets). Typically, only small amounts of the inactive cytochrome P420 forms of the enzymes were generated on reduction and CO-binding, indicating that the *E. coli*-expressed enzymes contained cysteinate-ligated heme iron and were relatively stable to the carbon monoxide-binding process.

(B) Binding of Other Inhibitors. Addition of other known heme ligands was shown to induce typical P450 spectral perturbations in CYP102A2 and CYP102A3. Saturation of the oxidized enzymes with imidazole induced shift of the Soret maximum to 422 nm, and similar spectral conversions were observed with the tighter-binding azole derivatives 1-phenylimidazole and ω-imidazolyldodecanoic acid, both of which also exhibit tight binding to P450 BM3 (*52*). All azoles displayed hyperbolic binding curves, from which apparent K_d values of 1330 ± 75 μM (513 ± 30 μM), 45.2 ± 7.6 μM (0.95 ± 0.10 μM), and 9.5 ± 1.9 μM (4.5 ± 0.2 μM) were determined for binding of imidazole, 1-phenylimidazole, and ω-imidazolyldodecanoic acid, respectively, for CYP102A2 (CYP102A3). Cyanide also bound the ferric heme iron, inducing a Soret shift to 438 nm. Binding was substantially weaker than with the azoles, with K_d values of 3.1 ± 0.7 mM (2.8 ± 0.3 mM) for CYP102A2 (CYP102A3). Addition of a few bubbles of nitric oxide (NO) gas to CYP102A2 and CYP102A3 resulted in the formation of an NO complex with the Soret band shifted to 433 nm and increased absorption of the α/β bands (with maxima at 573 and 540 nm, respectively) (Figure 3). These type II spectral shifts on addition of heme-ligating P450 inhibitors are highly similar to those observed previously with P450 BM3.

Cofactor and Cofactor Binding Properties. The carbonmonoxy and other adducts of CYP102A2 and CYP102A3 described above define the typical P450 heme system and coordination type. To further characterize the heme in these enzymes, we undertook electron paramagnetic resonance (EPR) studies of the two proteins in their oxidized forms. As expected, no signals typical of flavin radicals were observed in this state, but low-temperature X-band EPR studies of the P450's hemes revealed major signals constituting a rhombic trio of **g**-tensor elements. The occurrence of three major peaks in the EPR spectra for CYP102A2 and CYP102A3 indicates a nuclear spin state of $^1/_2$ in the hemes, as expected for ferric low-spin heme irons. The resulting *g*-values (g_z, g_y, and g_x) of 2.43, 2.26, and 1.92 for CYP102A2 and 2.42, 2.26, and 1.93 for CYP102A3 are highly similar to those recorded previously for both flavocytochrome P450 BM3 (2.41, 2.25, and 1.91) and its heme domain (2.42, 2.26, and 1.92) (*50*), and to those for the other well-characterized bacterial P450 system, P450cam (2.45, 2.26, and 1.91) (*53*).

Fluorescence spectroscopy was used to demonstrate the presence of flavins in the CYP102A2 and CYP102A3 enzymes. With fluorescence excitation at 450 nm, both samples produced fluorescence emission spectra with peaks near 540 nm, as expected for flavin-containing enzymes. To confirm the presence of both FAD and FMN cofactors in the enzymes, the fluorometric method of Forti and Sturani

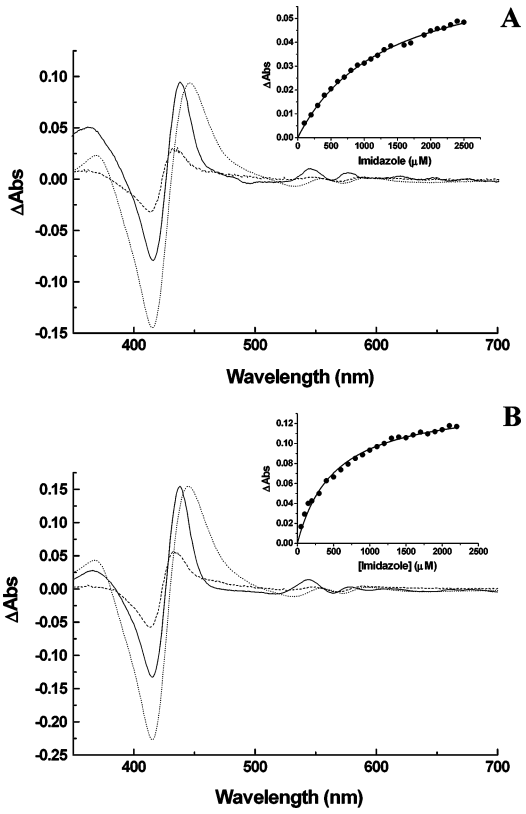

FIGURE 3: Inhibitor binding to CYP102A2 and CYP102A3. UV−visible absorption difference spectra are shown for the binding of saturating amounts of the inhibitors nitric oxide (solid line), imidazole (dashed line), and cyanide (dotted line) to 2 μM CYP102A2 (A) and 3.5 μM CYP102A3 (B). Insets show the fits of absorption change versus ligand concentration for the binding of imidazole to the P450s. Data are fitted to the Michaelis function to derive K_d values of 1330 ± 75 μM (CYP102A2) and 513 ± 30 μM (CYP102A3). Other inhibitor binding data are described in Binding of Other Inhibitors.

(as described by Aliverti et al.) was used (*54*, *55*). An approximately 10-fold enhancement of fluorescence was observed on phosphodiesterase treatment of the flavin-containing extract from CYP102A2 and CYP102A3 [obtained by boiling enzymes briefly in the dark, followed by cooling on ice and centrifugation to remove precipitated protein from the flavin-containing supernatant, as described (*55*)], indicating that both FAD and FMN cofactors are present in approximately stoichiometric amounts.

Binding of Fatty Acids. The tight binding of various long-chain saturated and unsaturated fatty acids to P450 BM3 has been demonstrated by several groups (e.g., *12*, *50*). Binding of fatty acids to P450 BM3 induces a shift in equilibrium of the heme iron spin state toward the high-spin form, leading to changes in the absorption spectrum in the Soret region (*12*). To determine whether fatty acids also bound CYP102A2 and CYP102A3, spectral binding titrations were performed for both enzymes with a range of saturated (lauric, myristic, palmitic, and stearic acids), unsaturated (arachidonic and linoleic acids), and branched-chain fatty acids (phytanic, 12-methylmyristic, 13-methylmyristic, 14-methylpentadecanoic, and 15-methylpalmitic acids). Arachidonic acid and the saturated fatty acids have been shown to be substrates for P450 BM3. Linoleic acid and phytanic acid were shown to dissociate the FatR repressor protein (located immediately upstream of the *cyp102A3* gene) from its operator, releasing

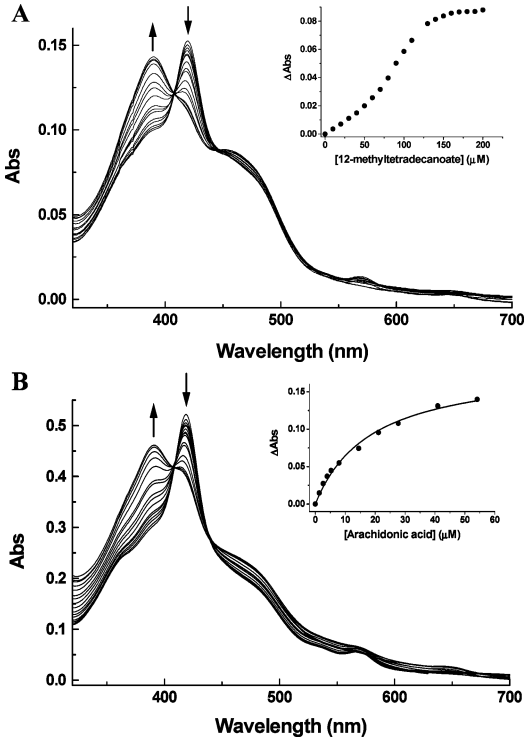

FIGURE 4: Fatty acid binding to CYP102A2 and CYP102A3. The spectral changes induced on titration of CYP102A2 (1.5 μM, panel A) with 12-methylmyristic acid (0−200 μM) and on titration of CYP102A3 (4.8 μM, panel B) with arachidonic acid (0−55 μM) are shown. Arrows indicate directions of change of spectra induced by successive additions of the substrates. In both cases, extensive conversion to the high-spin form of the enzymes is observed. Insets show the plots of fatty acid-induced absorption change computed from difference spectra generated by subtraction of the starting spectrum from subsequent spectra collected at each point in the titration. In both cases, A_{390} minus A_{420} data from the difference spectra are plotted versus the relevant [fatty acid]. The data plot for the titration of CYP102A2 with 12-methylmyristic acid is nonhyperbolic, but that for the titration of CYP102A3 with arachidonic acid does describe a hyperbola. A fit of these data to a rectangular hyperbola produces a K_d value of 18.5 ± 1.8 μM for the binding of arachidonic acid to CYP102A3.

repression of the *fatR-cyp102A3* operon (*56*). A variety of branched-chain fatty acids are prevalent in the membranes of *B. subtilis* and *B. megaterium* (e.g., *57*, *58*), but these molecules have not been tested systematically as substrates for the *Bacillus* P450s, despite their potential physiological relevance.

All fatty acids tested showed perturbation of the heme spectrum of both P450s, with shift of the resting (substrate-free, low-spin) Soret band from 418 nm toward a new position (at ~390 nm) typical of the high-spin forms (*50*). The extent of spin-state perturbation induced varied considerably between the different fatty acids tested, with far more extensive shifts in spin-state equilibrium observed for the unsaturated and branched-chain fatty acids than with the saturated fatty acids used. In particular, relatively small degrees of spin-state perturbation (<20%) were noted with lauric acid and stearic acid for CYP102A3 and for each of the four saturated straight-chain fatty acids with CYP102A2, within the solubility limits for these fatty acids in the aqueous buffer system. Figure 4 illustrates the spectral perturbations observed for CYP102A2 and CYP102A3 on titration with selected fatty acids. Plots of absorption change versus fatty acid concentration were hyperbolic in a number of cases (as for P450 BM3 with all fatty acids tested to date). However, the binding curves for various other fatty acids (most notably with the majority of the branched-chain lipids) were distinctly nonhyperbolic. While these data sets showed some sigmoidal characteristics, many could not be fitted accurately to the Hill function, suggesting that CYP102A2 and CYP102A3 are able to bind simultaneously two molecules of fatty acid substrates (with the sites having different affinities; see Discussion) but that the binding process does not reflect purely cooperative binding of more than one fatty acid molecule to the active sites of the enzymes (Figure 4, insets). The apparent binding constants, K_d values, for fatty acids to CYP102A2 and CYP102A3 are detailed in Table 2. CYP102A2 enzyme preparations with >80% heme content were used for all titrations reported in Table 2. However, comparative titrations with CYP102A2 preparations with lower heme content did not reveal any significant difference in behavior or apparent K_d values for fatty acids. An obvious observation is that both P450s bind the saturated fatty acids relatively weakly compared with the branched-chain and unsaturated fatty acids tested. Also of note is the relative similarity in K_d values between several of these fatty acids. This contrasts with P450 BM3 (and P450 BioI from *B. subtilis*), where there is a strong correlation between chain length and K_d values, at least for saturated fatty acids (e.g., *49*). In addition, although selected fatty acids do induce an almost complete change in the spin-state equilibrium of the heme iron in CYP102A2 and CYP102A3, none of the K_d values determined are as tight as those seen for P450 BM3 with substrates such as arachidonic, palmitic, and myristic acids (K_d values all in range 2−10 μM). A possible explanation for the rather lower affinities for the saturated fatty acids (cf. P450 BM3) is the absence of the Tyr/Arg motif at the mouth of the active site that is implicated in binding the carboxylate moiety of the substrates (*11*).

Reductase Activity and Pyridine Nucleotide Preference. Cytochrome P450 BM3 exhibits a strong preference for NADPH over NADH as the reducing substrate (*59*). In recent studies of P450 BM3 reductase-dependent steady-state reduction of cytochrome *c*, we have shown that the apparent K_M values for NADPH and NADH are 7.2 ± 0.3 μM and 12.8 ± 1.0 mM, respectively (*47*). To determine the relevant parameters for CYP102A2 and CYP102A3, we assayed the cytochrome *c* and ferricyanide reductase activities of these enzymes. The data detailed in Table 2 show that both enzymes catalyze rapid NADPH-dependent reduction of both substrates, with k_{cat} values comparable with those for P450 BM3. The K_M values for NADPH and NADH were determined in a series of assays in which NAD(P)H was varied at saturating concentrations of cytochrome *c*, and k_{obs} versus [NAD(P)H] data were fitted to a hyperbolic function. These data confirm that NADPH is the favored cofactor with K_M values of 3.6 ± 0.3 μM for CYP102A2 (cf. 17.9 ± 2.05 mM with NADH), and 5.1 ± 0.5 μM (cf. 2.43 ± 0.49 mM with NADH) for CYP102A3. CYP102A2 has higher apparent cytochrome *c* reductase activity than does CYP102A3, possibly as a result of a more efficient electron-transfer interaction site for this substrate.

Steady-State Fatty Acid Turnover. The steady-state turnover kinetics for CYP102A2 and CYP102A3 with the various fatty acids were determined by monitoring the fatty acid-dependent oxidation of NADPH at a saturating concentration

Table 2: Kinetic and Binding Parameters for the Interaction of CYP102A2 and CYP102A3 with Fatty Acids, Pyridine Nucleotides, and Electron Acceptors[a]

	CYP102A2			CYP102A3		
substrate	K_d/K* (μM)	k_{cat}/k_{max}* (min^{-1})	K_M/K_H* (μM)	K_d/K* (μM)	k_{cat}/k_{max}* (min^{-1})	K_M/K_H* (μM)
lauric acid	2310 ± 990	1615 ±94*	1990 ± 40*	87.8 ± 1.9	104 ± 7.7	165 ± 29.0
myristic acid	1065 ± 200	41 ± 8.2	640 ± 80*	106 ± 7.5	556 ± 110	542 ± 107
palmitic acid	482 ± 175	200 ± 27*	570 ± 20*	72.4 ± 3.2	676 ± 112	337 ± 67.6
stearic acid	281 ± 115	430 ± 81.7	38.8 ± 17.5	97.9 ± 5.6	374 ± 48.7	68.5 ± 12.8
phytanic acid	121 ± 21	5430 ± 1810	150 ± 37.6	100 ± 14.6	794 ± 74.8	28.7 ± 6.0
12-methylmyristic acid	89.9 ± 4.8*	4215 ± 100*	77.2 ± 1.4*	63.4 ± 1.6*	2055 ± 90*	69.1 ± 2.0*
13-methylmyristic acid	78.5 ± 4.1*	3865 ± 215*	57.8 ± 2.4*	65.1 ± 1.7*	2160 ± 60*	56.5 ± 1.4*
14-methylpentadecanoic acid	81.4 ± 5.7*	4790 ± 260*	51.0 ± 3.7*	53.1 ± 1.5*	2095 ± 57*	39.2 ± 1.4*
15-methylpalmitic acid	114 ± 11*	6105 ± 500	56.8 ± 11.1	62.6 ± 2.7	3845 ± 415	68.3 ± 15.9
linoleic acid	44.2 ± 1.5*	5230 ± 415*	50.2 ± 4.1*	25.8 ± 3.4	1110 ± 60*	43.2 ± 2.1*
arachidonic acid	40.2 ± 6.2*	6075 ± 285*	79.2 ± 6.1*	18.5 ± 1.8	1690 ± 200	79.0 ± 15.9
cytochrome *c*		11400 ± 180	6.9 ± 0.4		3520 ± 60	10.9 ± 0.8
ferricyanide		38150 ± 1850	153.4 ± 24.1		37050 ± 1000	285 ± 27
NADPH		11560 ± 200	3.6 ± 0.3		3530 ± 80	5.1 ± 0.5
NADH		1850 ± 100	17900 ± 2050		95.4 ± 6.1	2430 ± 485

[a] Apparent binding and kinetic constants (as described in Experimental Procedures) for interaction of CYP102A2 and CYP102A3 with various long-chain saturated, unsaturated, and branched-chain fatty acids are shown. For fatty acid binding constants determined from optical titration data, plots of absorption change versus [substrate] described either rectangular hyperbolae (from which K_d values were derived by fitting to a rectangular hyperbola) or were nonhyperbolic with sigmoidal characteristics. In the latter cases, apparent binding constants (K values) were approximated by fitting data to the Hill function (relevant K values are indicated by asterisks). For kinetic data, hyperbolic plots of reaction rate versus [substrate] were also fitted to the Michaelis function to derive k_{cat}/K_M parameters. Nonhyperbolic data (again having sigmoidal character) were again fitted to the Hill function to provide estimates of the apparent affinity (K_H) and rate constant (k_{max}) for these substrates. Results from kinetic data fitted in this way are again indicated by asterisks. The k_{cat} and K_M parameters for CYP102A2- and CYP102A3-dependent reduction of cytochrome *c* were derived by fitting data to the Michaelis function. The apparent K_M values for NADPH and NADH were determined from analysis of the dependence of cytochrome *c* reduction rate on [NAD(P)H] at saturating [cytochrome *c*]. Data were again fitted to the Michaelis function. Binding of the straight-chain fatty acids to CYP102A2 is relatively weak (by comparison with their low solubility in aqueous media), and extrapolation beyond the limits of the data points is required to obtain limiting values. For this reason, errors on these data sets are typically larger than those for the binding and turnover of other substrates with CYP102A2 and CYP102A3. The saturated fatty acids induce only small degrees of heme iron spin-state shift in the CYP102A2 enzyme, resulting in particularly large errors in these spectral binding data sets, all of which are fitted to rectangular hyperbolae within the accessible substrate solubility range.

of the pyridine nucleotide cofactor. Results are detailed in Table 2. Higher catalytic rates were generally observed with branched-chain and unsaturated fatty acids than with the saturated fatty acids used, in broad agreement with the higher affinity for these molecules determined from optical binding assays. CYP102A2 exhibited a higher rate of turnover of many of these substrates than did CYP102A3 (e.g., maximal turnover rates of 3865 ± 215 min^{-1}, cf. 2160 ± 60 min^{-1} with 13-methylmyristic acid) (Table 2). Analysis of peroxide production (by horseradish peroxidase-dependent reduction of *o*-dianisidine) indicated that there was <3% uncoupling of NADPH oxidation to peroxide in all of the reactions (*60*). Thus it appears that both enzymes are efficient and well-coupled fatty acid oxygenases, as is their close relative P450 BM3.

Plots of k_{obs} for CYP102A2/CYP102A3 versus fatty acid concentration were hyperbolic in the case of certain substrates (e.g., phytanic acid for both CYP102A2 and CYP102A3), enabling determination of the k_{cat}/K_M parameters by fitting to the Michaelis function. However, as observed in the optical binding assays with fatty acids, the dependence of reaction rate on fatty acid concentration was nonhyperbolic in the case of several of the lipids tested, particularly for a number of the branched-chain fatty acids. Figure 5 shows typical kinetic plots for CYP102A2/CYP102A3. As with the spectral binding data, many of the nonhyperbolic data sets showed sigmoidal characteristics but were not accurately fitted by the Hill function. However, reasonably accurate parameters for the half-saturation point with substrate (K) and the maximal rate constant (k_{max}) were obtained by fitting to a sigmoidal function, and these data are presented in Table 2.

Table 3: Distribution of Hydroxylated Products of Myristic Acid for P450 BM3, CYP102A2, and CYP102A3[a]

	position of myristic acid hydroxylation		
enzyme	ω-1 (%)	ω-2 (%)	ω-3 (%)
CYP102A1	54.6	24.9	20.4
CYP102A2	20.7	61.7	17.6
CYP102A3	10.5	46.8	42.6

[a] The proportions of ω-1, ω-2, and ω-3 products generated from myristic acid by the three different *Bacillus* flavocytochrome fatty acid oxygenases are shown. Data were generated as described in Experimental Procedures.

Analysis of Lipid Products. Previous studies on P450 BM3 have shown that this enzyme catalyzes efficient hydroxylation of myristic acid and other long-chain saturated fatty acids, with hydroxylation occurring exclusively at the ω-1, ω-2, and ω-3 positions. Hydroxylation of myristic acid occurs at the same carbon atoms for CYP102A2, CYP102A3, and P450 BM3, but the pattern of regioselectivity of hydroxylation of myristic acid is different for each enzyme. While P450 BM3 hydroxylates predominantly at the ω-1 position, the major product for CYP102A2 is the ω-2 hydroxy myristic acid, while CYP102A3 oxygenates mainly at the ω-2 and ω-3 positions, in approximately equal proportions (Table 3). While both *B. subtilis* flavocytochrome enzymes produced large amounts of hydroxylated products, their rate of consumption of myristic acid substrate was not as fast as that for P450 BM3. Samples taken after 20 min of reaction time showed that P450 BM3 had oxygenated 98%

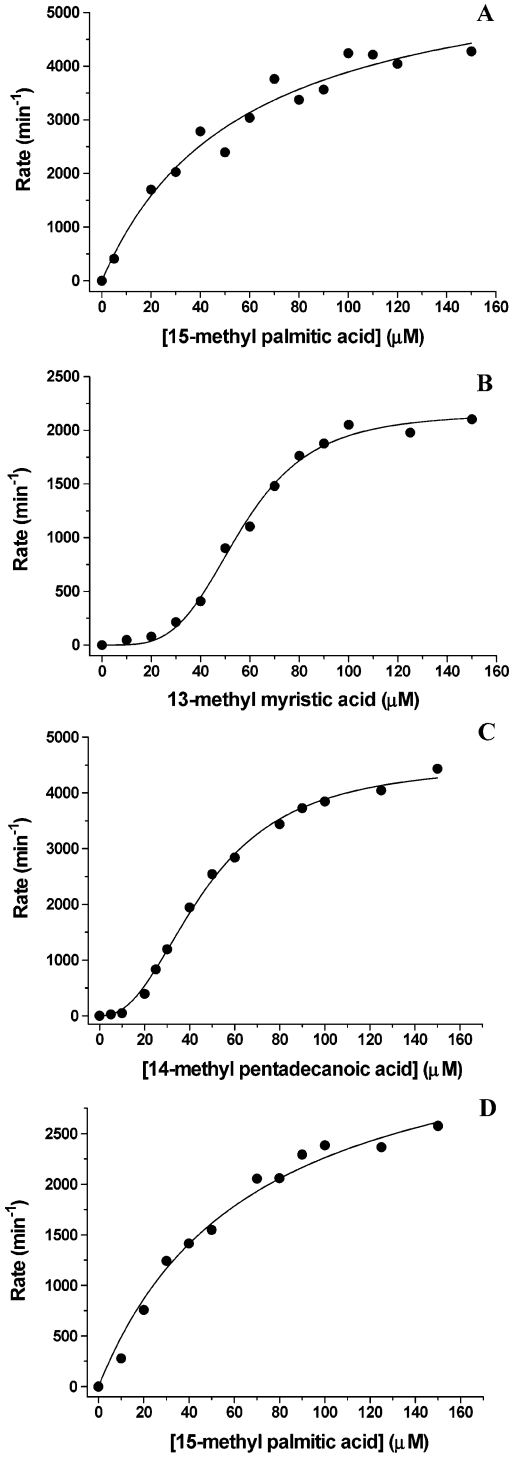

FIGURE 5: Steady-state turnover of fatty acids by CYP102A2 and CYP102A3. (A) Rate of NADPH oxidation catalyzed by CYP102A2 in the presence of varying concentrations of 15-methylpalmitic acid. Data are fitted to a rectangular hyperbola by use of Origin software, yielding parameters of $k_{cat} = 6105 \pm 500$ min^{-1} and $K_M = 56.8 \pm 11.1$ μM. (B) Comparable data set for CYP102A3 with 13-methylmyristic acid. The plot of rate versus [fatty acid] is nonhyperbolic and is fitted to the Hill function, producing parameters of $k_{max} = 2160 \pm 60$ min^{-1} and $K_H = 56.5 \pm 1.4$ μM. (C) Comparable set of data for turnover of 14-methylpentadecanoic acid by CYP102A2. Data are fitted to the Hill function producing parameters of $k_{max} = 4790 \pm 260$ min^{-1} and $K_H = 51.0 \pm 3.7$ μM. (D) Comparable set of data for turnover of 15-methylpalmitic acid by CYP102A3. Data are fitted to a rectangular hyperbola producing parameters of $k_{cat} = 3845 \pm 415$ min^{-1} and $K_M = 68.3 \pm 15.9$ μM. Kinetics were performed as described in Experimental Procedures.

of the substrate, while the proportions of myristic acid converted in the same time for CYP102A2 and CYP102A3 were approximately 25% and 89%, respectively. Leaving reactions to run for longer times resulted in essentially complete conversion of the fatty acid substrate to oxygenated products.

DISCUSSION

The P450 BM3 fatty acid hydroxylase system from *B. megaterium* has been one of the most intensively studied P450 enzymes in recent years (*14*). P450 BM3's high activity (resulting from fusion to a eukaryotic-like P450 reductase redox partner) and the pliability of its active site have stimulated much interest in exploitation of the enzyme for biotechnological purposes, e.g., stereo- and/or regioselective oxidations to generate high-value chemicals and pharmaceuticals. Despite intensive molecular characterization, the physiological role of P450 BM3 remains uncertain. Suggested functions include roles in sporulation or in metabolism of toxic fatty acids. The genes encoding both P450 BM3 and CYP102A3 are inducible by fatty acids (and a range of other molecules in the case of P450 BM3), which displace a repressor protein with binding site upstream of the *B. megaterium* CYP102A1 and *B. subtilis* CYP102A3 genes (*56*, *61*, *62*). However, studies on the regulation of the *B. subtilis* P450s indicate that an adaptive response to toxic linoleic acid was independent of the CYP102A2 and CYP102A3 systems (*56*). However, the subsequent discovery of genes encoding P450 BM3-like enzymes in other soil-dwelling bacteria (e.g., *Bacillus anthracis*, *Bradyrhizobium japonicum*, *Streptomyces avermitilis*, and *Ralstonia metallidurans*) suggests that this class of P450 does have important physiological functions and is more widespread in prokaryotes than was initially thought. Recently, a gene encoding a novel BM3-like enzyme was discovered in the maize pathogenic fungus *Gibberella moniliformis*, located in a gene cluster involved in biosynthesis of a fumonisin mycotoxin (*63*).

Despite high levels of sequence identity between P450 BM3 and CYP102A2/CYP102A3, there are intriguing differences in their properties with respect to fatty acid binding and turnover. For the long-chain saturated fatty acids tested (C_{12}, C_{14}, C_{16}, and C_{18}), the binding is generally substantially weaker and turnover rate considerably slower for CYP102A2/CYP102A3 with respect to P450 BM3 (Table 2). An exception is the interaction of lauric acid with CYP102A3, where apparent K_d/K_M values are comparable with those for P450 BM3, but in this case the k_{cat} value is at least 20-fold lower than for P450 BM3. The relatively weak binding of the straight-chain saturated fatty acids to CYP102A2 results in their inability to saturate the active site of the enzyme at the limits of their solubility in the aqueous buffer system used. The apparent kinetic and binding constants determined in these cases generally have rather larger errors associated, due to the requirement for extrapolation to reach the apparent limiting values. Notwithstanding these findings, both enzymes catalyzed efficient hydroxylation of myristic acid (Table 3). In contrast to the data with saturated substrates, steady-state turnover of many branched-chain fatty acids occurs with maximal rates comparable to those for P450 BM3 and its better substrates (*34*). For both CYP102A2 and CYP102A3, the best substrate tested (as regards k_{cat} values)

was 15-methylpalmitic acid (6105 ± 500 min^{-1} and 3845 ± 415 min^{-1}, respectively). Turnover rates for the branched-chain fatty acids were consistently higher for CYP102A2 than for CYP102A3. However, the relatively poor discrimination between binding of different substrates is evident from comparisons of the K_d/K_H values for the binding of the different branched-chain fatty acids (Table 2). For CYP102A2 these are in the range 78.5−121 μM, while for CYP102A3 the range is 53.1−100 μM. This apparent lack of discrimination extends to the interaction of saturated fatty acids with CYP102A3, although optical titration data indicate that the unsaturated fatty acids bind slightly more tightly to this P450 (Table 2). A feature of the interaction of P450 BM3 with its various fatty acid substrates is that there is a considerable discrimination between fatty acids of different chain length, with K_d and K_M values varying from ~200 μM for lauric acid (C_{12}) through to ~2 μM or less for the tightest binding saturated fatty acids (pentadecanoic acid and palmitic acid) and for certain unsaturated fatty acids (e.g. arachidonic acid; *36*). The relative lack of discrimination observed for CYP102A2 and CYP102A3 obviously relates to differences in active-site structure in these P450s compared to P450 BM3.

Changes in linker length and constitution with respect to P450 BM3 do not have great influence on interdomain electron transfer, since catalytic center activity of both CYP102A2 and CYP102A3 is rapid with the best substrates. The largest deviation in the whole amino acid sequence alignment of the three flavocytochromes occurs at the junction between the heme and flavin domains (in the region between amino acids 453 and 478 in Figure 1, right panel), with CYP102A2 having approximately seven additional amino acid residues in its linker with respect to CYP102A3 and P450 BM3. In recent years, there have been many efforts to engineer cytochrome P450/P450 reductase fusions with enhanced catalytic activity via improved interdomain electron transfer (reviewed in ref *3*). Examination of the different linker constitution in the highly related P450 BM3, CYP102A2, and CYP102A3 enzymes shows that large differences in linker constitution do not result in diminished catalytic efficiency. This may reflect that specific interactions between the FMN- and heme-binding domains are the major requirement for rapid electron transfer to the heme iron and that the linker serves only to tether the interacting domains in close proximity in order to increase the frequency of productive interactions.

Despite weaker binding of the saturated fatty acids with respect to P450 BM3, the three hydroxylated products obtained from CYP102A2- and CYP102A3-dependent turnover of the C_{14} substrate myristic acid are the same as those derived from P450 BM3: the ω-1, ω-2, and ω-3 monohydroxymyristic acids (Table 3). However, the precise regioselectivity of oxygenation varies between the enzymes. CYP102A2 hydroxylates myristic acid predominantly at the ω-2 position, while CYP102A3 favors the ω-3 carbon. This could reflect differing cellular requirements for the ω-2 and ω-3 metabolites, which might have specific signaling or other roles in this species. This could explain the requirement for two distinct flavocytochrome P450 enzymes in *B. subtilis*. An alternative explanation might be that the two enzymes fulfill a similar cellular role but are expressed at different growth stages. CYP102A2 may be under control of the σ-factor E, a sporulation-specific transcription factor (*64*), whereas CYP102A3 is induced as required when the substrate reaches sufficiently high endogenous levels to bind and displace the FatR repressor (*56*).

In conclusion, we have cloned, expressed, purified, and undertaken kinetic, spectroscopic, and binding studies of the CYP102A2 and CYP102A3 enzymes from *Bacillus subtilis*. Both enzymes are FAD-, FMN-, and heme *b*-containing flavocytochromes P450 that bind and hydroxylate fatty acids. However, there are intriguing differences with respect to the well-characterized P450 BM3 homologue, including large decreases in selectivity toward long-chain saturated fatty acids. In addition, there is nonhyperbolic binding and steady-state kinetic behavior with various branched-chain and unsaturated fatty acids, likely reflecting the binding of two molecules of these substrates in the active sites of the *B. subtilis* flavocytochromes. An alternative explanation could be that these enzymes are predominantly dimeric in solution (as P450 BM3 is considered to be) and that the binding of substrate to one monomer of the dimer influences the substrate K_d for the second monomer, giving rise to positive cooperativity. However, it should be noted that P450 BM3 itself has not been reported to exhibit sigmoidicity in substrate-binding or fatty acid oxidation kinetics. CYP102A2 consistently incorporates less heme than CYP102A3 in the *E. coli* expression system, but control experiments indicated that nonhyperbolic binding/kinetic curves are not a result of heme depletion in this enzyme. Co-binding of more than one substrate-like molecule in the P450 BM3 active site has been reported previously (*52*, *65*), but all fatty acids tested with this enzyme to date display apparent simple hyperbolic dependences for the binding and turnover of substrates. However, the atypical CYP102A2 and CYP102A3 kinetics have been recognized previously in other P450 systems and can be rationalized in terms of a two-site binding model, in which K_M and/or k_{cat} values are different for the substrates binding in the two sites (*66*, *67*). In the study by Korzekwa et al. (*66*), a variety of forms of P450 kinetic and binding curves are described according to the various apparent binding (K_{d1}, K_{d2}) and kinetic parameters (K_{M1}, K_{M2}, V_{max1}, V_{max2}) for the two substrate molecules bound. According to whether $K_{d1}/K_{M1} > K_{d2}/K_{M2}$ or vice versa, and dependent on the relative values of V_{max1} and V_{max2}, considerable deviations from hyperbolic binding/kinetic curves can be observed. In particular, the importance of the V_{max1} and V_{max2} parameters in determining the final form of the rate versus [substrate] curves means that it is feasible to obtain optical binding curves that resemble hyperbolae, while kinetic curves for the same substrate are clearly nonhyperbolic (e.g., for CYP102A3 with linoleic acid), or vice versa (e.g., for CYP102A2 with 15-methylpalmitic acid), in addition to observing similar forms for both binding and kinetic curves (e.g., CYP102A3 with palmitic acid) (*66*). The apparent K_d/K and K_M/K_H values are typically of similar magnitude, but variations are evident in certain cases and likely result from differences in the V_{max1} and V_{max2} parameters. It should also be remembered that the estimates of apparent binding constants (whether by fitting to a sigmoidal or hyperbolic function) obtained for CYP102A2 and CYP102A3 in most cases are saturation midpoints, with the true distinct K_d/K_M values for substrate binding in the two different sites impossible to discern accurately from these analyses. How-

ever, the deviations from "pure" hyperbolic dependence of reaction rate and/or heme iron spin-state change on [substrate] in several cases for CYP102A2 and CYP102A3 are strongly suggestive of bipartite substrate binding in these enzymes, as has been inferred in P450 BM3 on the basis of other evidence (e.g., *52*, *65*). Cooperativity of substrate binding (e.g. to enzyme monomers in a solution dimer) cannot be ruled out at this point, but titration curves in many cases do not fit well to the Hill function. It is tempting to speculate that the absence of the fatty acid carboxylate-binding motif defined by Tyr 51/Arg 47 in P450 BM3 is one of the determinants for the observed changes in kinetic and binding behavior for CYP102A2/CYP102A3. However, a Y51F mutant of P450 BM3 showed rather minor effects on substrate binding and kinetic properties. In addition, while a P450 BM3 R47A mutant and a R47A/Y51F double mutant showed compromised substrate binding and turnover properties, there was no deviation from hyperbolic binding and kinetic curves (*35*). Thus, it appears more likely that several subtle structural changes throughout the extended hydrophobic active sites in the heme domains of CYP102A2 and CYP102A3 (>35% of heme domain residues are different than those in P450 BM3) combine to alter the substrate binding modes in these enzymes and to produce the apparent nonhyperbolic dependence of kinetic and binding parameters on the substrate concentration. Ongoing studies on these enzymes include mutagenesis work to investigate structure/function relationships in CYP102A2/CYP102A3, with particular emphasis on those residues that vary from those recognized as catalytically important in preceding studies of P450 BM3. Such studies may reveal how differences in kinetic/binding properties of the *B. subtilis* flavocytochromes relate to specific amino acid variations from P450 BM3. However, the results of these studies can be best understood with reference to the atomic structures of the proteins. For this reason, attempts are underway to crystallize the CYP102A2 and CYP102A3 heme domains. We are also attempting to establish conditions for crystallization of the intact flavocytochromes. Preliminary studies indicate that the CYP102A3 enzyme is more stable in solution than is P450 BM3, with a lower tendency to aggregate and precipitate. These findings suggest that it may be feasible to crystallize and determine the structure of the intact CYP102A3 enzyme, enabling a better understanding of the interaction between the covalently linked P450 reductase and P450 domains in this important P450 class.

ACKNOWLEDGMENT

We are grateful to Professor Andrew Thomson at the University of East Anglia, Centre for Metalloprotein Spectroscopy and Biology, for access to facilities and helpful discussions.

REFERENCES

1. Nelson, D. R., Koymans, L., Kamataki, T., Stegeman, J. J., Feyereisen, R., Waxman, D. J., Waterman, M. R., Gotoh, O., Coon, M. J., Estabrook, R. W., Gunsalus, I. C., and Nebert, D. W. (1996) P450 superfamily: update on new sequences, gene mapping, accession numbers and nomenclature, *Pharmacogenetics 6*, 1−42.
2. Munro, A. W., and Lindsay, J. G. (1996) Bacterial cytochromes P-450, *Mol. Microbiol. 20*, 1115−1125.
3. Miles, C. S., Ost, T. W. B., Noble, M. A., Munro, A. W., and Chapman, S. K. (2000) Protein engineering of cytochromes P-450, *Biochim. Biophys. Acta 1543*, 383−407.
4. Von Wachenfeldt, C., and Johnson, E. F. (1995) In *Cytochrome P450: Structure, Mechanism and Biochemistry* (Ortiz de Montellano, P. R., Ed.) pp 183−223, Plenum Press, New York.
5. Poulos, T. L., Finzel, B. C., and Howard, A. J. (1986) Crystal structure of substrate-free *Pseudomonas putida* cytochrome P-450, *Biochemistry 25*, 5314−5322.
6. Williams, P. A., Cosme, J., Sridhar, V., Johnson, E. F., and McRee, D. E. (2000) Mammalian microsomal cytochrome P450 monooxygenase: structural adaptations for membrane binding and functional diversity, *Mol. Cell 5*, 121−131.
7. Von Wachenfeldt, C., Richardson, T. H., Cosme, J., and Johnson, E. F. (1997) Microsomal P450 2C3 is expressed as a soluble dimer in *Escherichia coli* following modification of its N-terminus, *Arch. Biochem. Biophys. 339*, 107−114.
8. Wester, M. R., Johnson, E. F., Marques-Soares, C., Dansette, P. M., Mansuy, D., and Stout, C. D. (2003) Structure of a substrate complex of mammalian cytochrome P450 2C5 at 2.3 Å resolution: evidence for multiple substrate binding modes, *Biochemistry 42*, 6370−6379.
9. Williams, P. A., Cosme, J., Ward, A., Angove, H. C., Matak Vinkovic, D., and Jhoti, H. (2003) Crystal structure of human cytochrome P450 2C9 with bound warfarin, *Nature 424*, 464−468.
10. Ravichandran, K. G., Boddupalli, S. S., Hasemann, C. A., Peterson, J. A., and Deisenhofer, J. (1993) Crystal structure of hemoprotein domain of P450 BM-3, a prototype for microsomal P450's, *Science 261*, 731−736.
11. Li, H.-Y., and Poulos, T. L. (1997) The structure of the cytochrome P450 BM-3 haem domain complexed with the fatty acid substrate, palmitoleic acid, *Nat. Struct. Biol. 4*, 140−146.
12. Narhi, L. O., and Fulco, A. J. (1987) Identification and characterization of two functional domains in cytochrome P-450 BM-3, a catalytically self-sufficient monooxygenase induced by barbiturates in *Bacillus megaterium*, *J. Biol. Chem. 262*, 6683−6690.
13. Peterson, J. A., Lorence, M. C., and Amarneh, B. (1990) Putidaredoxin reductase and putidaredoxin. Cloning, sequence determination, and heterologous expression of the proteins, *J. Biol. Chem. 265*, 6066−6073.
14. Munro, A. W., Leys, D., McLean, K. J., Marshall, K. R., Ost, T. W., Daff, S., Miles, C. S., Chapman, S. K., Lysek, D. A., Moser, C. C., Page, C. C., and Dutton, P. L. (2002) P450 BM3: the very model of a modern flavocytochrome, *Trends Biochem. Sci. 27*, 259−257.
15. Porter, T. D., and Coon, M. J. (1991) Cytochrome P-450. Multiplicity of isoforms, substrates, and catalytic and regulatory mechanisms, *J. Biol. Chem. 266*, 13469−13472.
16. Blattner, F. R., Plunkett, G., 3rd, Bloch, C. A., Perna, N. T., Burland, V., et al. (1997) The complete genome sequence of *Escherichia coli* K-12, *Science 277*, 1453−1553.
17. Arabidopsis genome initiative (2001) *Arabidopsis* could shed light on human genome, *Nature 410*, 299.
18. Cole, S. T., Brosch, R., Parkhill, J., Garnier, T., Churcher, C., et al. (1998) Deciphering the biology of *Mycobacterium tuberculosis* from the complete genome sequence, *Nature 393*, 537−544.
19. Souter, A., Mclean, K. J., Smith, W. E., and Munro, A. W. (2000) The genome sequence of *Mycobacterium tuberculosis* reveals cytochromes P450 as novel anti-TB drug targets, *J. Chem. Technol. Biotechnol. 75*, 933−941.
20. Kunst, F., Ogasawara, N., Moszer, I., Albertini, A. M., Alloni, G., et al. (1997) The complete genome sequence of the Gram-positive bacterium *Bacillus subtilis*, *Nature 390*, 249−256.
21. Von Wachenfeldt, C., and Hederstedt, L. (2002) in *Bacillus subtilis and Its Closest Relatives: From Genes to Cells* (Sonenshein, A. L., Hoch, J. A., and Losick, R., Eds.) pp 163−179, ASM Press, Washington, DC.
22. Green, A. J., Rivers, S. L., Cheesman, M. R., Reid, G. A., Quaroni, L. G., MacDonald, I. D. G., Chapman, S. K., and Munro, A. W. (2001) Expression, purification and characterization of cytochrome P450 BioI: a novel P450 involved in biotin synthesis in *Bacillus subtilis*, *J. Biol. Inorg. Chem. 6*, 523−533.
23. Stok, J. E., and De Voss, J. J. (2000) Expression, purification, and characterization of BioI: a carbon−carbon bond cleaving cytochrome P450 involved in biotin biosynthesis in *Bacillus subtilis*, *Arch. Biochem. Biophys. 384*, 351−360.

24. Cryle, M. J., Matovic, N. J., and De Voss, J. J. (2003) Products of cytochrome P450(BioI) (CYP107H1)-catalyzed oxidation of fatty acids, *Org. Lett. 5*, 3341−3344.
25. Matsunaga, I., Yamada, A., Lee, D. S., Obayashi, E., Fujiwara, N., Kobayashi, K., Ogura, H., and Shiro, Y. (2002) Enzymatic reaction of hydrogen peroxide-dependent peroxygenase cytochrome P450s: kinetic deuterium isotope effects and analyses by resonance Raman spectroscopy, *Biochemistry 41*, 1886−1892.
26. Lee, D. S., Yamada, A., Sugimoto, H., Matsunaga, I., Ogura, H., Ichihara, K., Adachi, S., Park, S. Y., and Shiro, Y. (2003) Substrate recognition and molecular mechanism of fatty acid hydroxylation by cytochrome P450 from *Bacillus subtilis*. Crystallographic, spectroscopic, and mutational studies, *J. Biol. Chem. 278*, 9761−9767.
27. Daff, S., Ingledew, W. J., Reid, G. A., and Chapman, S. K. (1996) New insights into the catalytic cycle of flavocytochrome b_2, *Biochemistry 35*, 6345−6350.
28. Taylor, P., Pealing, S. L., Reid, G. A., Chapman, S. K., and Walkinshaw, M. D. (1999) Structural and mechanistic mapping of a unique fumarate reductase, *Nat. Struct. Biol. 6*, 1108−1112.
29. Poole, R. K., and Hughes, M. N. (2000) New functions for the ancient globin family: bacterial responses to nitric oxide and nitrosative stress, *Mol. Microbiol 36*, 775−83.
30. Narhi, L. O., and Fulco, A. J. (1986) Characterization of a catalytically self-sufficient 119,000-dalton cytochrome P-450 monooxygenase induced by barbiturates in *Bacillus megaterium*, *J. Biol. Chem. 261*, 7160−7169.
31. Marletta, M. A., Hurshman, A. R., and Rusche, K. M. (1998) Catalysis by nitric oxide synthase, *Curr. Opin. Chem. Biol. 2*, 656−663.
32. Kitazume, T., Takaya, N., Nakayama, N., and Shoun, H. (2000) *Fusarium oxysporum* fatty-acid subterminal hydroxylase (CYP505) is a membrane-bound eukaryotic counterpart of *Bacillus megaterium* cytochrome P450 BM3, *J. Biol. Chem. 275*, 39734−39740.
33. Hoch, J. A. (1991) Genetic analysis in *Bacillus subtilis*, *Methods Enzymol. 204*, 305−320.
34. Studier, F. W., and Moffat, B. A. (1986) Use of bacteriophage T7 RNA polymerase to direct selective high-level expression of cloned genes, *J. Mol. Biol. 189*, 113−130.
35. Hanahan, D., Jessee, J., and Bloom, F. R. (1991) Plasmid transformation of *Escherichia coli* and other bacteria, *Methods Enzymol. 204*, 63−113.
36. Noble, M. A., Miles, C. S., Chapman, S. K., Lysek, D. A., Mackay, A. C., Reid, G. A., Hanzlik, R. P., and Munro, A. W. (1999) Roles of key active-site residues in flavocytochrome P450 BM3, *Biochem. J. 339*, 371−379.
37. Omura, T., and Sato, R. (1964) The carbon monoxide-binding pigment of liver microsomes. I. Evidence for its hemoprotein nature, *J. Biol. Chem. 239*, 2370−2378.
38. Aliverti, A., Curti, B., and Vanoni, M. (1999) Identifying and quantitating FAD and FMN in simple and in iron−sulfur-containing flavoproteins, *Methods Mol. Biol. 131*, 9−23.
39. M^{c}Lean, K. J., Cheesman, M. R., Rivers, S. L., Richmond, A., Leys, D., Chapman, S. K., Reid, G. A., Price, N. C., Kelly, S. M., Clarkson, J., Smith, W. E., and Munro, A. W. (2002) Expression, purification and spectroscopic characterization of the cytochrome P450 CYP121 from *Mycobacterium tuberculosis*, *J. Inorg. Biochem. 91*, 527−541.
40. Capdevila, J. H., Wei, S. Z., Helvig, C., Falck, J. R., Belosludtsev, Y., Truan, G., Graham-Lorence, S. E., and Peterson, J. A. (1996) The highly stereoselective oxidation of polyunsaturated fatty acids by cytochrome P450 BM-3, *J. Biol. Chem. 271*, 22663−22671.
41. Oliver, C. F., Modi, S., Sutcliffe, M. J., Primrose, W. U., Lian, L. Y., and Roberts, G. C. K. (1997) A single mutation in cytochrome P450 BM3 changes substrate orientation in a catalytic intermediate and the regiospecificity of hydroxylation, *Biochemistry 36*, 1567−1572.
42. Munro, A. W., Malarkey, K., McKnight, J., Thomson, A. J., Kelly, S. M., Price, N. C., Lindsay, J. G., Coggins, J. R., and Miles, J. S. (1994) The role of tryptophan 97 of cytochrome P450 BM3 from *Bacillus megaterium* in catalytic function. Evidence against the 'covalent switching' hypothesis of P-450 electron transfer, *Biochem. J. 303*, 423−428.
43. Ost, T. W. B., Miles, C. S., Munro, A. W., Murdoch, J., Reid, G. A., and Chapman, S. K. (2001) Phenylalanine 393 exerts thermodynamic control over the heme of flavocytochrome P450 BM3, *Biochemistry 40*, 13421−13429.
44. Ost, T. W. B., Miles, C. S., Murdoch, J., Cheung, Y., Reid, G. A., Chapman, S. K., and Munro, A. W. (2000) Rational re-design of the substrate binding site of flavocytochrome P450 BM3, *FEBS Lett. 486*, 173−177.
45. Maves, S. A., Yeom, H., McLean, M. A., and Sligar, S. G. (1997) Decreased substrate affinity upon alteration of the substrate-docking region in cytochrome P450 BM-3, *FEBS Lett. 414*, 213−218.
46. Shen, A. L., Sem, D. S., and Kasper, C. B. (1999) Mechanistic studies on the reductive half-reaction of NADPH-cytochrome P450 oxidoreductase, *J. Biol. Chem. 274*, 5391−5398.
47. Roitel, O., Scrutton, N. S., and Munro, A. W. (2003) Electron transfer in flavocytochrome P450 BM3: kinetics of flavin reduction and oxidation, the role of cysteine 999, and relationships with mammalian cytochrome P450 reductase, *Biochemistry 42*, 10809−10821.
48. Klein, M. L., and Fulco, A. J. (1993) Critical residues involved in FMN binding and catalytic activity in cytochrome P450 BM-3, *J. Biol. Chem. 268*, 7553−7561.
49. Sanger, F., Nicklen, S., and Coulson, A. R. (1977) DNA sequencing with chain-terminating inhibitors, *Proc. Natl. Acad. Sci. U.S.A. 74*, 5463−5467.
50. Miles, J. S., Munro, A. W., Rospendowski, B. N., Smith, W. E., McKnight, J., and Thomson, A. J. (1992) Domains of the catalytically self-sufficient cytochrome P-450 BM-3. Genetic construction, overexpression, purification and spectroscopic characterization, *Biochem. J. 288*, 503−509.
51. Daff, S., Chapman, S. K., Turner, K. L., Holt, R. A., Govindaraj, S., Poulos, T. L., and Munro, A. W. (1997) Redox control of the catalytic cycle of flavocytochrome P-450 BM3, *Biochemistry 36*, 13816−13823.
52. Noble, M. A., Quaroni, L., Chumanov, G. D., Turner, K. L., Chapman, S. K., Hanzlik, R. P., and Munro, A. W. (1998) Imidazolyl carboxylic acids as mechanistic probes of flavocytochrome P-450 BM3, *Biochemistry 37*, 15799−15807.
53. Tsai, R., Yu, C. A., Gunsalus, I. C., Peisach, J., Blumberg, W., Orme-Johnson, W. H., and Beinert, H. (1970) Spin-state changes in cytochrome P-450cam on binding of specific substrates, *Proc. Natl. Acad. Sci. U.S.A. 66*, 1157−1163.
54. Forti, G., and Sturani, E. (1968) On the structure and function of reduced nicotinamide adenine dinucleotide phosphate-cytochrome *f* reductase of spinach chloroplasts, *Eur. J. Biochem. 3*, 461−472.
55. Aliverti, A., Curti, B., and Vanoni, M. A. (1999) Identifying and quantitating FAD and FMN in simple and iron−sulfur-containing flavoproteins, *Methods Mol. Biol. 131*, 9−23.
56. Gustafsson, M. C. U., Palmer, C. N. A., Wolf, C. R., and Von Wachenfeldt, C. (2001) Fatty-acid-displaced transcriptional repressor, a conserved regulator of cytochrome P450 102 transcription in *Bacillus* species, *Arch. Microbiol. 176*, 459−464.
57. Rilfors, L., Wieslander, A., and Stahl, S. (1978) Lipid and protein composition of membranes of *Bacillus megaterium* variants in the temperature range 5 to 70 degrees C, *J. Bacteriol. 135*, 1043−1052.
58. Kaneda, T. (1991) Iso- and anteiso-fatty acids in bacteria: biosynthesis, function, and taxonomic significance, *Microbiol. Rev. 55*, 288−302.
59. Narhi, L. O., Wen, L. P., and Fulco, A. J. (1988) Characterization of the protein expressed in *Escherichia coli* by a recombinant plasmid containing the *Bacillus megaterium* cytochrome P-450 BM-3 gene, *Mol. Cell. Biochem. 79*, 63−71.
60. Macheroux, P., Massey, V., Thiel, D. J., and Volokita, M. (1991) Expression of spinach glycolate oxidase in *Saccharomyces cerevisiae*: purification and characterization, *Biochemistry 30*, 4612−4619.
61. Fulco, A. J. (1991) P450 BM-3 and other inducible bacterial P450 cytochromes: biochemistry and regulation, *Annu. Rev. Pharmacol. Toxicol. 31*, 177−203.
62. Lee, T. R., Tsu, H. P., and Shaw, G. C. (2001) Transcriptional regulation of the *Bacillus subtilis* bscR-CYP102A3 operon by the BscR repressor and differential induction of cytochrome CYP102A3 expression by oleic acid and palmitate, *J. Biochem. (Tokyo) 130*, 569−574.
63. Proctor, R. H., Brown, D. W., Plattner, R. D., and Desjardins, A. E. (2003) Coexpression of 15 contiguous genes delineates a fumonisin biosynthetic gene cluster in *Gibberella moniliformis*, *Fungal Genet. Biol. 38*, 237−249.
64. Feucht, A., Evans, L., and Errington, J. (2003) Identification of sporulation genes by genome-wide analysis of the sigmaE regulon of *Bacillus subtilis*, *Microbiology 149*, 3023−3034.

65. Rock, D. A., Perkins, B. N., Wahlstrom, J., and Jones, J. P. (2003) A method for determining two substrates binding in the same active site of cytochrome P450 BM3: an explanation of high energy omega product formation, *Arch. Biochem. Biophys. 416*, 9−16.
66. Korzekwa, K. R., Krishnamarchary, Shou, M., Ogai, A., Parise, R. A., Rettie, A. E., Gonzalez, F. J., and Tracy, T. S. (1998) Evaluation of atypical cytochrome P450 kinetics with two-substrate models: evidence that multiple substrates can simultaneously bind to cytochrome P450 active sites, *Biochemistry 37*, 4137−4147.
67. Houston, J. B., and Kenworthy, K. E. (2000) *In vitro-in vivo* scaling of CYP kinetic data not consistent with the classical Michaelis−Menten model, *Drug Met. Dispos. 28*, 246−254.

BI035904M